Optics Letters

Ferris wheel patterning of Rydberg atoms using electromagnetically induced transparency with optical vortex fields

Hamid R. Hamedi,[1,*] Viačeslav Kudriašov,[1] Ning Jia,[2] Jing Qian,[3] and Gediminas Juzeliūnas[1]

[1]Institute of Theoretical Physics and Astronomy, Vilnius University, Saulėtekio 3, Vilnius LT-10257, Lithuania
[2]The Public Experiment Center, University of Shanghai for Science and Technology, Shanghai 200093, China
[3]State Key Laboratory of Precision Spectroscopy, Quantum Institute for Light and Atoms, Department of Physics, School of Physics and Electronic Science, East China Normal University, Shanghai 200062, China
*Corresponding author: hamid.hamedi@tfai.vu.lt

Received 9 April 2021; revised 5 July 2021; accepted 17 July 2021; posted 21 July 2021 (Doc. ID 427000); published 24 August 2021

We study the formation of spatially dependent electromagnetically induced transparency (EIT) patterns from pairs of Laguerre–Gauss (LG) modes in an ensemble of cold interacting Rydberg atoms. The EIT patterns can be generated when two-photon detuning does not compensate for the Rydberg level energy shift induced by van der Waals interaction. Depending on the topological numbers of each LG mode, we can pattern dark and bright Ferris-wheel-like structures in the absorption profile with tunable barriers between sites, providing confinement of Rydberg atoms in transverse direction while rendering them transparent to light at specific angular positions. We also show how the atomic density may affect the azimuthal modulation of the absorption profile.

https://doi.org/10.1364/OL.427000

Coherent control of atom–light interaction has important applications in quantum and nonlinear optics. Quantum coherence induced by interaction of laser radiation and atoms results in a number of appealing effects [1–7]. Electromagnetically induced transparency (EIT) [6,7] is a quantum interference effect where the destructive interference between probability amplitudes of two optical transitions leads to the elimination of absorption and an associated steep variation of the refractive index around the resonant frequency [6]. In its simplest form, EIT requires only three atomic levels and two light beams in a suitable atomic medium with a Λ configuration geometry.

Using Rydberg atoms, one can apply the EIT for nonlinear quantum optics at low light intensities [8]. Because of their extreme polarizability and long-range interactions, Rydberg atoms with highly excited principal quantum numbers provide applications in precision electrometry [9] and quantum information [10]. Since the van der Waals (vdWs) interaction between the atoms is enhanced with the principal quantum number, the interaction between Rydberg atoms is much larger than the interaction between atoms in their ground states [8,11].

Optical vortex beams with helical wavefronts carry an orbital angular momentum (OAM) [12]. Apart from many other interesting effects [13–17], the interaction of optical vortices with atoms leads to narrowing of the EIT spectral width [18] and allows one to azimuthally modulate the optical susceptibility of a medium, and create spatially dependent EIT patterns [19–21]; the latter has potential applications in high capacity optical data storage and continuous variable quantum technologies [19].

Previous scenarios for patterning spatially dependent EIT structures required closed-loop atom–light coupling [19–21]. The spatially dependent EIT in [19–21] is due to the quantum interference between the probe and control fields carrying a single OAM component. In this paper, this is realized by coupling the Rydberg atoms in a ladder configuration (non-closed loop) by a control field that is the superposition of two Laguerre–Gauss (LG) modes carrying arbitrary OAMs. Such a scheme is not sensitive by itself to the phase of the control field in the same way as the closed-loop scenarios proposed in [19–21]; rather, the OAM dependence originates from the dependence of the susceptibility on the squared magnitude of the control field. Note that when two vortex beams, each carrying an optical vortex, are superimposed, the resulting beam develops new vortices depending on the OAM of each vortex component [16,22]. Such a light field has been employed for trapping cold and quantum degenerate atomic samples [17,23,24]. Here we are interested in the absorption of a plane wave representing a probe beam coupling lower levels of the ladder scheme of Rydberg atoms influenced by two LG control beams carrying OAM. Due to the interference of the constituting LG field, the probe absorption becomes dependent on the azimuthal angle and the corresponding OAM, producing specific EIT absorption and transparency patterns exhibiting spatial Ferris-wheel-type structures with azimuthal symmetry. Such a model effectively converts optical phase information into intensity information and may find potential applications in storage of high-dimensional optical information in phase dependent quantum memories [19] as well as in creation of various ring traps for quantum degenerate gasses [23]. We stress that such

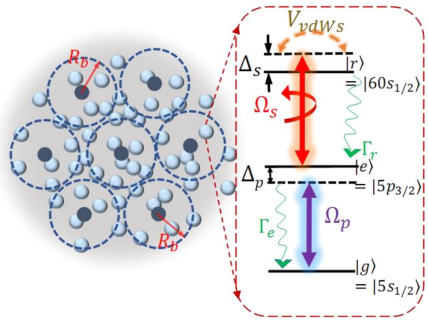

Fig. 1. Schematic representation of an atomic ensemble composed of blocked Rydberg superatoms coupled by a superposition beam of two optical vortices $\Omega_s(r,\phi)=\Omega_{s1}(r,\phi)+\Omega_{s2}(r,\phi)$ and a weak nonvortex probe field Ω_p. Here Δ_p and Δ_s denote detunings of the probe and coupling field from the corresponding atomic transition frequencies, respectively; R_b is the blockade radius within which only a single atom can be excited to the uppermost Rydberg state.

a scheme can be realized with non-Rydberg atoms. However, the strong interatomic interaction makes the compensation for two-photon detuning easier at wider specific angular positions, allowing one to obtain sharper spatially dependent EIT patterns for Rydberg atoms at other places where the two-photon detuning is not compensated for by the Rydberg interaction.

We consider an ensemble of Rydberg atoms characterized by a typical three-level ladder configuration of energy levels as illustrated in Fig. 1. For each atom, the ground, excited, and highly excited Rydberg states are characterized by state-vectors $\{|g\rangle,|e\rangle,|r\rangle\}$, respectively. A weak probe field with the Rabi frequency Ω_p acts on the lower transition $|g\rangle-|e\rangle$ of the ladder, while the upper transition $|e\rangle-|r\rangle$ is coupled by a stronger control field that is a superposition of two equally polarized co-propagating LG vortex fields $\Omega_s(r,\phi)=\Omega_{s1}(r,\phi)+\Omega_{s2}(r,\phi)$ [23], with their Rabi frequencies $\Omega_{sk}(r,\phi)=|\Omega_{sk}(r)|e^{il_k\phi}$ $(k=1,2)$, where l_k denotes OAM (topological charge). Corresponding amplitudes for the case of a doughnut LG beam with the waist w and strength ε_k read $|\Omega_{sk}(r)|=\varepsilon_k(\frac{r}{w})^{|l_k|}e^{-r^2/w^2}$. The probe field is considered a plane wave with the Rabi frequency $\Omega_p=|\Omega_p|=\varepsilon_p$ independent of the transverse coordinates.

Here we assume a cloud of dense frozen Rydberg gas where the center-of-mass motion of the atoms is negligible on the time scale of the experiment [25]. The Hamiltonian of the system under the rotating wave and electric dipole approximations is then given by $(\hbar=1)$ $\mathcal{H}=\mathcal{H}_a+\mathcal{V}_{af}+\mathcal{V}_{vdWs}$, with the unperturbed atomic Hamiltonian $\mathcal{H}_a=-\sum_j^N[\Delta_p\sigma_{ee}^j+(\Delta_s+\Delta_p)\sigma_{rr}^j]$, atom–field interaction $\mathcal{V}_{af}=-\sum_j^N[\Omega_p\sigma_{eg}^j+\Omega_s\sigma_{re}^j+\text{H.c.}]$, and inter-nuclear vdWs type interaction $\mathcal{V}_{vdWs}=\sum_{j<m}^N\frac{C_6}{|\mathbf{r}_j-\mathbf{r}_m|^6}\sigma_{rr}^j\otimes\sigma_{rr}^m$. Here $\sigma_{\alpha\beta}^j=|\alpha\rangle\langle\beta|_j$ shows the transition operator $(\alpha\neq\beta)$ or projection operator $(\alpha=\beta)$, and C_6 characterizes the vdWs coefficient, which depends on $|r\rangle$. When the size of the atom is of the same order as the wavelength of light, dipole approximation may not be sufficient. However, if the beam waist is much larger than the size of the Rydberg atom, this approximation may be still valid. Otherwise, we would have a large field gradient across the Rydberg atom, and dipole approximation will not be valid. We also note that the dipole approximation may hold good for Rydberg atoms in the case of photoionization occurring in the vicinity of the nucleus [26]. One can adopt a superatom strategy to replace $\mathcal{V}_{vdWs}$ with $\sum_j^N\sigma_{rr}^j\sum_{m\neq j}\frac{C_6}{|\mathbf{r}_j-\mathbf{r}_m|^6}\sigma_{rr}^m$ under the mean-field treatment [27], by which the many-body interacting system is replaced by a model of one atom j affected by the accumulated level shifts from other nearby excited atoms. For short excitation times, this method yields good agreement with experiments [28]. For the jth atom, the time evolution of the operator $\sigma_{\alpha\beta}^j(t)$ is governed by the Heisenberg equations of motion that have the same form as in [29]. In the equations, $s=\sum_{m\neq j}\frac{C_6}{|\mathbf{r}_j-\mathbf{r}_m|^6}\sigma_{rr}^m$ characterizes vdWs-induced energy shift for the atom j created by the adjacent Rydberg-state atoms m, and $\gamma_{\alpha\beta}=(\Gamma_\alpha+\Gamma_\beta)/2$ denotes the dephasing rate, with $\alpha,\beta\in(g,e,r)$. The dominant contribution to the dephasing is coming from the interaction among Rydberg atoms, i.e., γ_{er}, which is much larger than other dephasings. The decay rates obey the condition $\Gamma_e\gg\Gamma_r$, $\Gamma_g\approx 0$, so $\gamma=\gamma_{er}=\gamma_{ge}$, $\Gamma_e=2\gamma$, and $\gamma_{gr}=\Gamma_r\approx 0$. Hereafter superscript j will be ignored for the sake of simplicity.

The probe absorption $\sigma_{ge}^I=\text{Im}(\sigma_{ge})$ can be derived by solving the system of motion equations under the steady limit $(\dot{\sigma}_{\alpha\beta}(t)=0)$. In what follows, we assume $\Delta_p\approx 0$. Then Δ_s actually stands for two-photon detuning, and the absorption simplifies to [29]

$$\sigma_{ge}^I=\frac{\gamma_{ge}(\Delta_s-s)^2\Omega_p}{(I_p+I_s)^2+(\Delta_s-s)^2(\gamma_{ge}^2+2I_p)}. \tag{1}$$

In this case, one has a relation of the energy shifts to the Rydberg state s (magnitude of the approximated vdWs interaction) [5] $s\approx\frac{\omega}{\xi}\sigma_{rr}=\frac{\omega}{\xi}\frac{I_p(I_p+I_s)}{(I_p+I_s)^2+(\Delta_s-s)^2(\gamma_{ge}^2+2I_p)}$. Here $I_{p,s}=|\Omega_{p,s}|^2$ represent intensities of the probe and control fields, γ_{ge} is the dephasing rate of a $|g\rangle$-$|e\rangle$ transition, and ξ is an adjustable parameter controlled by the atomic density. The latter is expressed as $\xi=(R/R_b)^3$, where R is the interatomic distance, and R_b is Rydberg blockade radius, which can be found as $R_b=\sqrt[6]{C_6/\omega}$, where C_6 is the vdWs interaction constant, and ω is the half-linewidth of a line shape of s. As can be seen from Eq. (1), in the case of $\Delta_s=s$ (perfect anti-blockade), the absorption is always zero due to the EIT. To study the absorption characteristics unaffected by the anti-blockade regime, we will restrict our study to the case of $\Delta_s\neq s$, specifically taking $s\ll\Delta_s$.

In our simulations, we take the characteristic parameters of the atomic ^{87}Rb gas: spontaneous decay rate $\Gamma_e=2\pi\cdot 6.1$ MHz, transition dephasing rate $\gamma_{ge}=\Gamma_e/2$, vdWs constant $C_6=2\pi\cdot 1.4\cdot 10^{11}$ μm^6/s. We use corresponding detunings $\Delta_s=2\Gamma_e$ and $\Delta_p=0$. The typical atomic density is $\rho=5\cdot 10^{10}$ cm^{-3}. We also assume the strengths of the both vortex control fields to be equal, i.e., $\varepsilon_1=\varepsilon_2=\varepsilon_s$. As typical control and probe Rabi frequencies, we take $\varepsilon_s=\Gamma_e$ and $\varepsilon_p=0.1\Gamma_e$, respectively. Note that the latter parameters will be subject to variation in the course of our analysis. The steady-state limit is reasonable here because the time for steady state $\tau\sim 5$ μs is much longer than the intermediate state's lifetime Γ_e^{-1} under condition $\varepsilon_s/\varepsilon_p=10$ [5]. During the steady-state period τ, a rough estimation for the thermal motion of atoms gives a distance of $\Delta R=v\tau\approx 200$ nm if the most probable

velocity is $v \sim 4$ cm/s at $T = 20$ μK. Since the average interatomic distance $R = (3/4\pi\rho)^{1/3} \sim 2\ \mu\text{m} \gg \Delta R$, it is then safe to ignore the atomic center-of-mass motion.

In what follows, we are interested in the spatial dependence of the absorption profile $\sigma_{ge}^{I}(r, \phi)$, which comes from $I_s = I_s(r, \phi)$ and $s = s(r, \phi)$ spatial dependencies and is based on the transversely inhomogeneous control field $\Omega_s(r, \phi)$. Expanding $I_s = |\Omega_{s1} + \Omega_{s2}|^2 = (|\Omega_{s1}| \cos(l_1\phi) + |\Omega_{s2}| \cos(l_2\phi))^2 + (|\Omega_{s1}| \sin(l_1\phi) + |\Omega_{s2}| \sin(l_2\phi))^2$, one can see a direct dependence of Eq. (1) on OAM numbers l_1 and l_2. This indicates that the absorption of the probe field depends on the OAM numbers of the individual LG beams.

We start with a general analysis of Eq. (1) by discussing the nonlinear absorption properties of the Rydberg EIT system. First, we do so by studying absorption σ_{ge}^{I} dependence on the control field amplitudes ε_s (Fig. 2) without taking into account any transverse dependence of the control fields' driving upper $|e\rangle$-$|r\rangle$ transition. One can see a strong nonlinear dependence of σ_{ge}^{I} against ε_s in the figure. In the given probe strength range $\varepsilon_p \lesssim 0.1\Gamma_e$, the absorption is monotonically decreasing with increasing the control strength, indicating a decrease in medium's absorption (increase of transparency). The absorption is less significant at smaller values of the probe field strength ε_p. The strengths $\varepsilon_p \lesssim 0.1\varepsilon_s$ are used to meet the EIT conditions, which would be violated when the strengths ε_p and ε_s become of comparable values.

Next, by taking into consideration the spatial structure of the control fields, we model the characteristic distributions of the absorption profiles in the case of non-equal $|l_2| \neq |l_1|$ and equal opposite $l_2 = -l_1$ topological charges (Figs. 3 and 4). (The case of equal $l_2 = l_1$ is trivial and thus not presented here.) In these figures, the bright points in the absorption profiles represent low light transmission (high absorption), while the dark points correspond to regions of optical transparency (low absorption).

For $|l_2| \neq |l_1|$, the absorption profiles shown in Fig. 3 have different types of angular rotation symmetry with the angle $\Delta\phi = 2\pi/|\Delta l|$ determined by the OAM number difference $\Delta l = l_2 - l_1$. This type of symmetry corresponds well to the intensity profile of a two-OAM-component control beam where interference between vortices forms central and peripheral singularities (not shown here) [16]. These singularities lead to high absorption areas seen as bright spots in the plots (bright

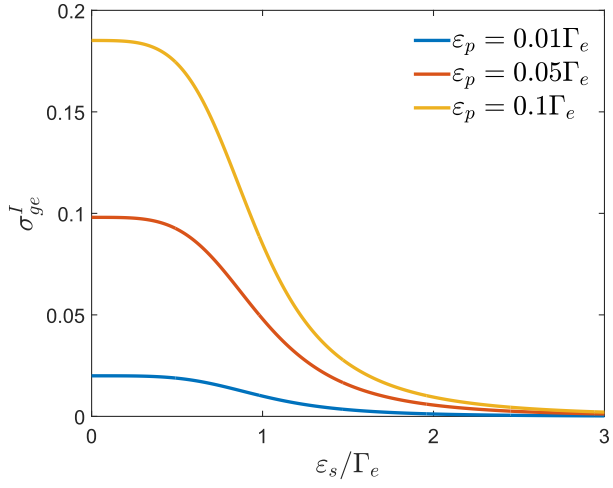

Fig. 2. Optical absorption σ_{ge}^{I} as a function of control field strength ε_s for different probe field strengths ε_p.

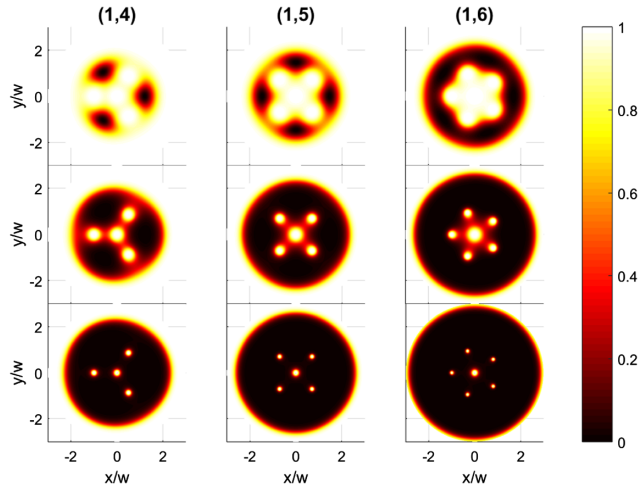

Fig. 3. Normalized absorption [Eq. (1)] distributions for the increasing control field strengths $\varepsilon_s = 1\Gamma_e$, $\varepsilon_s = 3\Gamma_e$, and $\varepsilon_s = 7\Gamma_e$ (from top to bottom row) and different OAM number combinations denoted by pairs of numbers (l_1, l_2) (from left to right columns). Other parameters are $\varepsilon_p = 0.1\Gamma_e$ and $\Delta_s = 2\Gamma_e$.

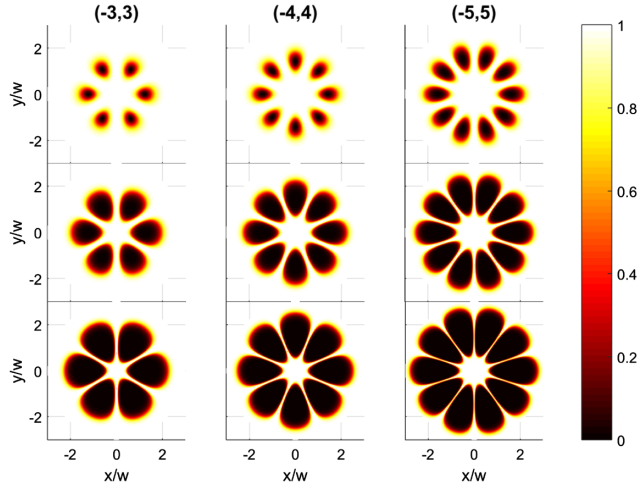

Fig. 4. Normalized absorption [Eq. (1)] distributions for increasing control field strengths $\varepsilon_s = 1\Gamma_e$, $\varepsilon_s = 3\Gamma_e$, and $\varepsilon_s = 7\Gamma_e$ (from top to bottom row) and different OAM number combinations denoted by pairs of numbers (l_1, l_2). Other parameters are $\varepsilon_p = 0.1\Gamma_e$ and $\Delta_s = 2\Gamma_e$.

Ferris wheels). Notably, we can see that the increase in control field strength also leads to shrinking of the absorption zones and development of sharp distinct absorption sites on the transparent background. Overall, the transparency area due to the EIT expands as the control field intensity increases.

In the case of Fig. 4 where $l_1 = -l_2 = |l|$, the absorption pattern develops a rather different structure that has an azimuthal dependence governed by $2\cos(|l|\phi)$. A sort of dark Ferris wheels structure with a $2|l|$ symmetry is formed (flower-like "petals" pattern of dark color). As in the previous case, the control strength increase leads to shrinking of the absorption areas between petals; however, as the composite beam interference pattern contains no peripheral singularities, it does not form distinct low-light transmission sites in the absorption structure, but rather leads to an extended and merged absorption area on

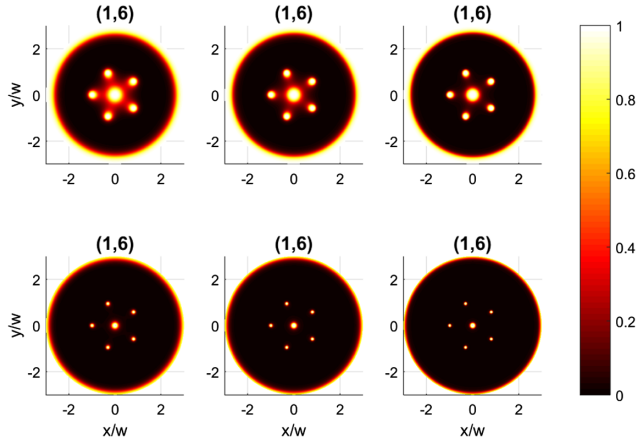

Fig. 5. Normalized absorption [Eq. (1)] distributions for increasing values of the atomic density ρ (from left to right): 0.05, 0.15, and 0.25 μm^{-3} and different values of field strengths: $\varepsilon_s = 3\Gamma_e$ (top row), $\varepsilon_s = 7\Gamma_e$ (bottom row). Other parameters used: $\varepsilon_p = 0.1\Gamma_e$ and $\Delta_s = 2\Gamma_e$.

which the petal-type EIT transparency structure is visible (dark Ferris wheels).

Finally, we consider the dependence of absorption on the atomic density for fixed amplitudes of probe and control fields. The absorption dependence on density comes from parameter s depending on $\xi(\rho)$. The increase in ρ reduces interatomic separation R, which in turn leads to the decrease in ξ and increase in s, which becomes comparable to Δ_s resulting in $\sigma_{ge}^{I} \to 0$. Parameter s has linear dependence on density: $s(\rho) \sim \xi^{-1} \sim \rho$. In our case, the working point is at the value of $\rho = 0.05\ \mu m^{-3}$, and we consider a regime where $s \ll \Delta_s$, as at higher values of atomic density, the anti-blockade regime is approached. As presented in Fig. 5, in the given density range ($\rho \leq 0.25$), for the case of unequal OAMs, there is a weak increase in sharpness of absorption sites with density. The effect is barely visible, and higher density values may lead to sharper spatially dependent EIT patterns; however, in that case, the assumption of $s \ll \Delta_s$ becomes no longer valid.

In summary, we have studied the azimuthal dependence of EIT in a Rydberg atomic scheme subjected to a weak probe beam as well as control fields of larger intensity with OAMs. When two-photon detuning is not compensated for by the Rydberg level energy shift induced by the vdWs interaction, the probe absorption depends on the azimuthal angle and the OAM of the control vortex beams. We have considered different cases of absorption with different OAM number combinations of the control field components, leading to formation of bright and dark Ferris wheels, and also investigated the absorption dependence on atomic density ρ. The proposal allows for patterning Rydberg atoms at specific positions in azimuthal space, enabling single-site addressability of trapped arrays of atoms. In this way, optical ring lattice structures with strong confinement at each lattice point may be obtained [4].

Funding. European Social Fund (09.3.3-LMT-K-712-19-0031); National Natural Science Foundation of China (11474094); Science and Technology Commission of Shanghai Municipality (18ZR1412800).

Acknowledgment. We are particularly grateful to Julius Ruseckas for stimulating discussions. This work has received funding from European Social Fund (Project No. 09.3.3-LMT-K-712-19-0031) under grant agreement with the Research Council of Lithuania (LMTLT) for H.R.H.

Disclosures. The authors declare no conflicts of interest.

Data Availability. Data underlying the results presented in this paper are not publicly available at this time but may be obtained from the authors upon reasonable request.

REFERENCES

1. Y. Wu, J. Saldana, and Y. Zhu, Phys. Rev. A **67**, 013811 (2003).
2. Y. Niu and S. Gong, Phys. Rev. A **73**, 053811 (2006).
3. Y. Wu and L. Deng, Phys. Rev. Lett. **93**, 143904 (2004).
4. G. S. Agarwal and K. T. Kapale, J. Phys. B **39**, 3437 (2006).
5. T. Kirova, N. Jia, S. H. Asadpour, J. Qian, G. Juzeliūnas, and H. R. Hamedi, Opt. Lett. **45**, 5440 (2020).
6. M. Fleischhauer, A. Imamoglu, and J. P. Marangos, Rev. Mod. Phys. **77**, 633 (2005).
7. E. Paspalakis and P. L. Knight, Phys. Rev. A **66**, 015802 (2002).
8. D. Petrosyan, J. Otterbach, and M. Fleischhauer, Phys. Rev. Lett. **107**, 213601 (2011).
9. M. G. Bason, M. Tanasittikosol, A. Sargsyan, A. K. Mohapatra, D. Sarkisyan, R. M. Potvliege, and C. S. Adams, New J. Phys. **12**, 065015 (2010).
10. T. A. Johnson, E. Urban, T. Henage, L. Isenhower, D. D. Yavuz, T. G. Walker, and M. Saffman, Phys. Rev. Lett. **100**, 113003 (2008).
11. A. K. Mohapatra, T. R. Jackson, and C. S. Adams, Phys. Rev. Lett. **98**, 113003 (2007).
12. L. Allen, M. Padgett, and M. Babiker, *IV the Orbital Angular Momentum of Light* (Elsevier, 1999), pp. 291–372.
13. V. E. Lembessis and M. Babiker, Phys. Rev. A **82**, 051402 (2010).
14. D.-S. Ding, Z.-Y. Zhou, B.-S. Shi, X.-B. Zou, and G.-C. Guo, Opt. Lett. **37**, 3270 (2012).
15. J. Ruseckas, A. Mekys, and G. Juzeliūnas, Phys. Rev. A **83**, 023812 (2011).
16. H. R. Hamedi, J. Ruseckas, E. Paspalakis, and G. Juzeliūnas, Phys. Rev. A **99**, 033812 (2019).
17. V. E. Lembessis, A. Lyras, and O. M. Aldossary, J. Opt. Soc. Am. B **38**, 233 (2021).
18. V. S. Chauhan, R. Kumar, D. Manchaiah, P. Kumar, and R. K. Easwaran, Laser Phys. **30**, 065203 (2020).
19. N. Radwell, T. W. Clark, B. Piccirillo, S. M. Barnett, and S. Franke-Arnold, Phys. Rev. Lett. **114**, 123603 (2015).
20. S. Sharma and T. N. Dey, Phys. Rev. A **96**, 033811 (2017).
21. H. R. Hamedi, V. Kudriašov, J. Ruseckas, and G. Juzeliūnas, Opt. Express **26**, 28249 (2018).
22. I. D. Maleev and G. A. Swartzlander, J. Opt. Soc. Am. B **20**, 1169 (2003).
23. S. Franke-Arnold, J. Leach, M. J. Padgett, V. E. Lembessis, D. Ellinas, A. J. Wright, J. M. Girkin, P. Öhberg, and A. S. Arnold, Opt. Express **15**, 8619 (2007).
24. A. S. Arnold, Opt. Lett. **37**, 2505 (2012).
25. A. Browaeys, D. Barredo, and T. Lahaye, J. Phys. B **49**, 152001 (2016).
26. S. E. Anderson and G. Raithel, Nat. Commun. **4**, 2967 (2013).
27. T. E. Lee, H. Häffner, and M. C. Cross, Phys. Rev. A **84**, 031402 (2011).
28. H. Weimer, R. Löw, T. Pfau, and H. P. Büchler, Phys. Rev. Lett. **101**, 250601 (2008).
29. D. Ma, D. Yu, X.-D. Zhao, and J. Qian, Phys. Rev. A **99**, 033826 (2019).